Evaluation of Hemispheric Asymmetries in Marine Cloud Radiative Properties

FRIDA A.-M. BENDER AND ANDERS ENGSTRÖM

Department of Meteorology, and Bolin Centre for Climate Research, Stockholm University, Stockholm, Sweden

ROBERT WOOD AND ROBERT J. CHARLSON

Department of Atmospheric Science, University of Washington, Seattle, Washington

(Manuscript received 31 March 2016, in final form 1 February 2017)

ABSTRACT

The hemispheric symmetry of albedo and its contributing factors in satellite observations and global climate models is evaluated. The analysis is performed on the annual mean time scale, on which a bimodality in the joint distribution of albedo and cloud fraction is evident, resulting from tropical and subtropical clouds and midlatitude clouds, respectively. Hemispheric albedo symmetry is not found in individual ocean-only latitude bands; comparing the Northern and Southern Hemisphere (NH and SH), regional mean albedo is higher in the NH tropics and lower in the NH subtropics and midlatitudes than in the SH counterparts. This follows the hemispheric asymmetry of cloud fraction. In midlatitudes and tropics the hemispheric asymmetry in cloud albedo also contributes to the asymmetry in total albedo, whereas in the subtropics the cloud albedo is more hemispherically symmetric. According to the observations, cloud contributions to compensation for higher clear-sky albedo in the NH come primarily from cloud albedo in midlatitudes and cloud amount in the subtropics. Current-generation climate models diverge in their representation of these relationships, but common features of the model–data comparison include weaker-than-observed asymmetry in cloud fraction and cloud albedo in the tropics, weaker or reversed cloud fraction asymmetry in the subtropics, and agreement with observed cloud albedo asymmetry in the midlatitudes. Models on average reproduce the NH–SH asymmetry in total albedo over the 60°S–60°N ocean but show higher occurrence of brighter clouds in the SH compared to observations. The albedo bias in both hemispheres is reinforced by overestimated clear-sky albedo in the models.

1. Introduction

Albedo is the primary determinant of the amount of shortwave (SW) radiation absorbed by the earth–atmosphere system, and temporal and spatial variability of albedo are to first order driven by variability in cloud fraction (Loeb et al. 2007; George and Wood 2010; Engström et al. 2015). The relationship between albedo α and cloud fraction f can therefore be used to diagnose SW cloud radiative properties and their representation in models. Specifically, the derivative of albedo with respect to cloud fraction (i.e., the local slope $d\alpha/df$) is related to cloud albedo α_{cld}, as for a given clear-sky albedo α_{clr}, an increase in cloud fraction will give a greater increase in total albedo for a higher cloud optical depth.

Corresponding author e-mail: Frida Bender, frida@misu.su.se

Assuming a separation between clear-sky and cloud albedo (Cess 1976), the relation between albedo and cloud fraction can be described as

$$\alpha = \alpha_{\mathrm{cld}} f + \alpha_{\mathrm{clr}}(1 - f), \tag{1}$$

from which the cloud albedo can be derived as

$$\alpha_{\mathrm{cld}} = d\alpha/df + \alpha_{\mathrm{clr}}. \tag{2}$$

It should be noted that these equations rely on the definition of a fractional cloud cover f. Such a definition is not unambiguous, and even among observations it depends on a number of assumptions related to detection thresholds, sampling, and spatial resolution, as discussed in detail by, for example, Pincus et al. (2012), Stubenrauch et al. (2013), and Chepfer et al. (2013). The relation described by Eq. (1), however, is found to be a useful approximation for both regional and near-global

DOI: 10.1175/JCLI-D-16-0263.1

scale. Similar reasoning has been used by Nam et al. (2012) to show that the optical thickness of low clouds in the tropics and subtropics is overestimated in many global climate models and by Bender et al. (2011) to show that in subtropical stratocumulus regions, monthly mean cloud albedo does not vary notably with cloud fraction.

Engström et al. (2015) elucidated the nonlinear relationship between albedo and cloud fraction on the monthly mean time scale, for the near-global ocean, illustrating how total albedo as well as its sensitivity to cloud fraction increases with increasing cloud fraction. Here we study the same near-global cloud distribution on the annual mean time scale, which invites a separation of cloud regimes based on latitude (tropics, subtropics, and midlatitudes, here defined as 0°–20°, 20°–40°, and 40°–60° latitude, respectively) and accentuates differences between climate models and satellite observations, allowing a finer scrutiny of hemispheric differences in climate models.

On this annual time scale we then study differences in cloud radiative properties between the Northern and Southern Hemisphere (NH and SH). Satellite observations have indicated symmetry between the hemispheres in terms of average albedo (i.e., that the NH and SH mean albedo are practically the same; Vonder Haar and Suomi 1971; Voigt et al. 2013). This symmetry is not unanimously represented in climate models, and models from phases 3 and 5 of the Coupled Model Intercomparison Project (CMIP3 and CMIP5) display both negative and positive differences between NH and SH albedo (Voigt et al. 2013; Stephens et al. 2015).

As the NH has larger land area, contributing to higher surface albedo, the observed symmetry suggests that the SH has more cloud reflection, balancing the difference in surface albedo. Cloud adjustments to hemispheric asymmetries in absorbed energy have been demonstrated in idealized model simulations. For instance, Voigt et al. (2014) used aquaplanet simulations to show that artificial albedo perturbations cause shifts in the intertropical convergence zone (ITCZ) and related clouds, toward the hemisphere with lower albedo, counteracting the forced asymmetry. Along the same lines, Hwang and Frierson (2013) have argued that a shortage of cloud amount and cloud reflection in the Southern Ocean, also found by Trenberth and Fasullo (2010) in CMIP3 models, drives CMIP5 models to ITCZ migration toward the SH, contributing to the double-ITCZ problem afflicting many global models (Lin 2007; Oueslati and Bellon 2015). More recent studies by Kay et al. (2016) and Hawcroft et al. (2017), however, have found such teleconnections to have limited influence in model simulations incorporating a fully coupled ocean, highlighting the role of oceanic cross-equatorial heat transport.

Still, in general terms the SH would be expected to have more and/or brighter clouds than the NH, to compensate for the higher surface albedo in the NH, and produce the observed hemispheric symmetry. Here we provide a more detailed investigation of the degree of hemispheric asymmetry in cloud fraction, total albedo, and cloud albedo in CMIP5 models compared to satellite observations, on the annual mean time scale, making use of the abovementioned separation into tropics, subtropics, and midlatitudes. To isolate the role of clouds and avoid effects of land surface and sea ice contributions to albedo, we focus on clouds over ocean only and limit the study area to 60°S–60°N, noting that this neglects potentially important compensational effects of clouds over land and at high latitudes. Therefore we do not further investigate the higher-latitude Southern Ocean, which has previously been pointed out as a region with too little cloud reflection in the CMIP5 ensemble (Hwang and Frierson 2013), largely attributable to model shortcomings in simulating supercooled liquid in clouds (Bodas-Salcedo et al. 2016; McCoy et al. 2016; Kay et al. 2016).

We first evaluate differences between climate models and satellite observations (described in section 2) without separating the hemispheres, demonstrating the use of annual mean time scale and separation into latitude bands (section 3a), then show hemispheric differences (section 3b), and finally separate latitude bands in NH and SH (section 3c), analyzing the relation between albedo and cloud fraction as well as their regional mean values. Discussion and conclusions are given in section 4.

2. Models and observations

We analyze 26 global climate models participating in CMIP5 (Taylor et al. 2012) that provide monthly mean top-of-the-atmosphere (TOA) SW radiative fluxes and cloud fraction estimates. The models are listed in Table 1. The historical simulations considered incorporate natural and anthropogenic forcing, including solar irradiance, land-use changes, and emissions and concentrations of greenhouse gases and aerosols, and we study the 25-yr time period from 1980 to 2004, when the historical simulations end. The temporal overlap with the observational data is only partial, but the results are found to be insensitive to the choice of time period in the models.

TABLE 1. CMIP5 models considered in the study, and the institutions providing output. Models are numbered in agreement with the display order in Figs. 2–4. (Expansions of acronyms are available online at http://www.ametsoc.org/PubsAcronymList.)

No.	Model name	Institution
1	ACCESS1.0	CSIRO–BoM
2	ACCESS1.3	
3	BCC_CSM1.1	BCC
4	BNU-ESM	College of Global Change and Earth System Science (GCESS)
5	CanESM2	CCCma
6	CCSM4	NCAR
7	CESM1(CAM5)	NSF–DOE–NCAR
8	CNRM-CM5	CNRM–CERFACS
9	GFDL CM3	NOAA/GFDL
10	GFDL-ESM2G	
11	GFDL-ESM2M	
12	GISS-E2-R	NASA GISS
13	HadGEM2-CC	Met Office Hadley Centre [MOHC; additional realizations by the National Institute for Space Research (INPE), Brazil]
14	HadGEM2-ES	
15	INM-CM4.0	Institute of Numerical Mathematics (INM)
16	IPSL-CM5A-LR	IPSL
17	IPSL-CM5A-MR	
18	IPSL-CM5B-LR	
19	MIROC-ESM-CHEM	MIROC
20	MIROC-ESM	
21	MIROC4h	
22	MIROC5	
23	MPI-ESM-LR	Max Planck Institute for Meteorology (MPI-M)
24	MRI-CGCM3	MRI
25	NorESM1-M	Norwegian Climate Centre (NCC)
26	NorESM1-ME	

Observations of TOA radiative fluxes and of cloud fraction are taken from the Clouds and the Earth's Radiant Energy System (CERES; Wielicki et al. 1996) and the Moderate Resolution Imaging Spectroradiometer (MODIS; Barnes et al. 1998), respectively. The CERES and MODIS instruments are both carried on the polar-orbiting *Terra* and *Aqua* satellites, with equator-crossing times of 1030 and 1330 LT, respectively. Following Engström et al. (2015), we take the mean of observations from *Aqua* and *Terra*, during the period for which they overlap (i.e., July 2002 through April 2015), using the Single Scanner Footprint TOA/Surface Fluxes and Clouds (SSF) level-2, edition-3 product, which includes both radiative fluxes and associated cloud properties. Cloud properties are derived from five channels in the visible and infrared wavelengths, as described in Minnis et al. (2008, 2011), and radiative fluxes are determined using angular distribution models described in Loeb et al. (2005), assuming constant meteorology at satellite overpass time to derive diurnally varying fluxes from instantaneous values. The MODIS pixel size at nadir is 250–1000 m depending on wavelength, and the CERES footprint is 20 km. The observational data are analyzed on a $1^\circ \times 1^\circ$ resolution grid where each grid box includes the CERES footprints whose center falls within the given region, and the cloud fraction is given by the ratio of MODIS pixels determined to be cloudy to the total number of pixels in the region. Although it would be possible to allow for partly cloudy pixels, as in Coakley et al. (2005), this is not adopted within the standard MODIS products, and 1-km pixels are treated as fully cloudy or clear.

The comparison between models and observations is performed on the annual mean time scale, taking temporal averages of monthly mean albedo and cloud fraction data. Regional and hemispheric mean albedo is calculated as the ratio between area-weighted mean incoming and outgoing SW fluxes. We note that the satellite observations are based on limited sampling of the diurnal cycle, whereas the model output is based on full diurnal averages. This may lead to biases in magnitude and variability of albedo as well as cloud fraction. It is found, however, that replacing the current SSF satellite dataset with the synoptic radiative fluxes and clouds (SYN) dataset, which uses higher-frequency radiance measurements from geostationary satellites in the interpolation between CERES observations, does not affect the conclusions drawn from the model–data comparison.

We also note that the definition of cloud fraction may be different in models and observations, in terms of detection thresholds and overlap assumptions, and that satellite retrievals may be afflicted with observational limitations and artifacts (Marchand et al. 2010; Pincus et al. 2012; Stubenrauch et al. 2013). The observational cloud fraction used here was optimized to be consistent with the CERES radiation measurements and to detect clouds with greatest impact on the radiation budget. Although this cloud fraction dataset does not share the feature of excluding partly cloudy pixels, which creates a low bias in the MODIS cloud fraction data based on successful cloud optical properties retrievals, it does underestimate cloud amount, particularly in the tropical regions compared to other datasets including the standard MODIS cloud mask [see Platnick et al. (2003) for a description of MODIS cloud products and Pincus et al. (2012) and Minnis et al. (2008) for comparative evaluations]. This underestimate of cloud amount is attributed to a failure to detect optically thin clouds, and we also note that all MODIS-derived cloud fraction estimates

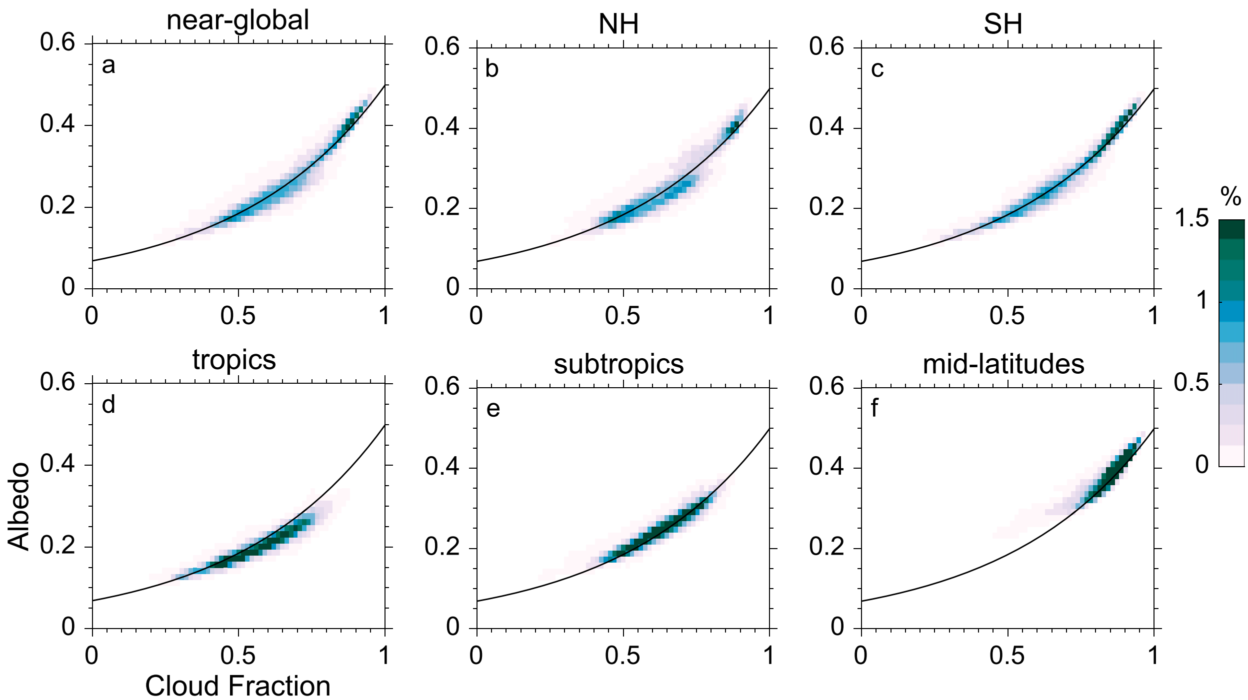

FIG. 1. Frequency of occurrence of each annually averaged observed (CERES and MODIS) cloud fraction–albedo combination, in percent of all cases in the given region, for (a) near-global region (60°S–60°N), (b) NH (0°–60°N), (c) SH (0°–60°S), (d) tropics (20°S–20°N), (e) NH and SH subtropics (20°–40°N and 20°–40°S), and (f) NH and SH midlatitudes (40°–60°N and 40°–60°S). Black lines represent an exponential fit to the near-global (60°S–60°N) satellite data, given by $\alpha = e^{(1.988f - 2.6832)}$.

underestimate the fraction of optically thin clouds compared to active sensors, including the lidar on *CALIPSO* (Winker et al. 2009), as discussed by Minnis et al. (2008). Quantitative comparison of cloud fraction may be aided by the use of satellite simulators (Bodas-Salcedo et al. 2011; Pincus et al. 2012); that is, model output simulating what a satellite would see if the clouds of the atmosphere were like those of the given model. This allows for a more direct comparison of both cloud fraction and cloud optical depth distribution of clouds in models and observations, as undertaken by, for example, Klein et al. (2013). However, the CMIP5 archive does not contain model output specifically simulating MODIS observations. Furthermore, satellite simulators cannot resolve all differences between actual retrievals and model-simulated clouds, and uncertainties in simulator output remain to be quantified (Pincus et al. 2012). One way to bypass the differences in cloud detection is to only consider clouds with optical thickness above a certain threshold. In the present study, however, the focus is not on a quantitative comparison of cloud fraction representation but on the relation between albedo and cloud fraction and its hemispherical asymmetry in models and observations. These relationships are not expected to be affected by possible systematic biases in cloud fraction between models and observations. For these reasons, the present analysis is based on the total albedo and the total given cloud fraction estimates from each model and for the combination of CERES and MODIS observations.

3. Results

a. *Annual mean joint distributions of albedo and cloud fraction*

Figure 1a shows the joint distribution of annual mean satellite-estimated total albedo and cloud fraction over the ocean between 60°S and 60°N. Similar to the monthly mean data from which they are derived (Engström et al. 2015), the annual mean data fall on a well-defined, nonlinear curve, although averaging over 12-month periods significantly reduces the variability. Further, the annual mean time scale indicates a bimodal distribution, in contrast with the more even distribution of monthly mean data. As seen in Fig. 1a, the data create one maximum with lower cloud fraction and lower albedo and one with higher cloud fraction and higher

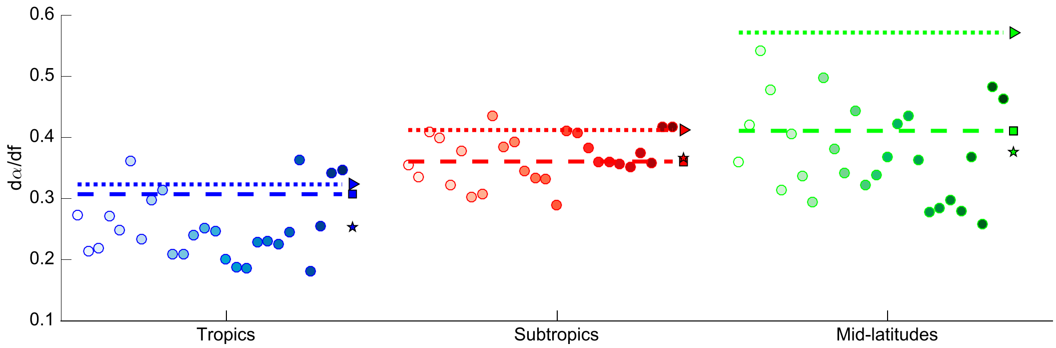

FIG. 2. Partial linear slopes $d\alpha/df$ for three latitude bands (both hemispheres) corrected for SZA dependence, according to Fig. A1. Tropics (0°–20°), subtropics (20°–40°), and midlatitudes (40°–60°) are represented by blue, red, and green colors, respectively. CMIP5 models listed in Table 1 are represented by circles, and stars indicate multimodel means. Squares and dashed lines indicate observations. Triangles and dotted lines indicate observations without applied correction for SZA dependence.

albedo. The two separable populations can be identified as originating from tropical and subtropical clouds and midlatitude clouds, respectively, as seen in Figs. 1d–f. Figures 1d–f also illustrate how the nonlinear relation on the near-global scale can be seen as a composite of pieces of more linear relationships in more restricted regions on the annual mean time scale. We note that on the monthly mean time scale large geographical regions like these display greater variability and less linearity (Bender et al. 2011).

The nonlinearity in albedo α with cloud fraction f (i.e., steeper slope $d\alpha/df$) at higher f (Fig. 1a) suggests higher cloud optical depth at higher cloud fraction, and Figs. 1d–f suggest that both f and $d\alpha/df$ are higher at higher latitude. This covariation between latitude, cloud fraction, and optical depth is also borne out in cloud optical depth retrievals from MODIS. However, noting that albedo as well as cloud optical depth retrievals are dependent on solar zenith angle (SZA) and viewing zenith angle (VZA) (Loeb and Davies 1996; Liang and Di Girolamo 2013; Cronin 2014), we use a radiative transfer model (RTM) [based on Corti and Peter (2009) and Cronin (2014)] to account for the part of the slope increase resulting from larger SZA at higher latitudes, as described in appendix A. In the following, the partial linear slopes and clear-sky albedos given for each region are adjusted using the enhancement factor for the mean SZA of that latitude band (as indicated in Fig. A1). We note that the spatial structure of the clouds may still cause deviations from the plane-parallel assumption of the RTM, such that low solar elevation at high latitudes may cause clouds to appear brighter than their plane-parallel model counterparts, and vice versa for low latitudes, in a way that cannot be accounted for without a three-dimensional RTM (Barker et al. 1999).

Figure 2 shows that in the observations there is an increase in slope $d\alpha/df$ with latitude, even when the SZA-induced increase is accounted for, suggesting that the higher-latitude clouds have higher optical thickness. We note here that the CERES SYN dataset (see section 2) indicates an even greater increase in slope with latitude, with a 10% larger midlatitude $d\alpha/df$ than given by the SSF data.

Corresponding to Fig. 1a, Fig. 3 displays the annual mean near-global distribution of points in albedo–cloud fraction space in 26 global models. In the models, as in the observations, albedo increases with cloud fraction but the models in general show larger variability in albedo for a given cloud fraction. The model distributions are with few exceptions shifted compared to the observations in a way that indicates too-high total albedo for a given cloud fraction. A comparison between the CERES SSF and SYN products (see section 2) indicates that the limited temporal sampling in the satellite observations may contribute to this bias; the near-global average cloud fraction is higher (relative difference 3%, 99% significant), and the near-global average albedo is lower (relative difference 1%, 99% significant) according to SSF compared with SYN, with local deviations on the order of 10%. In the relation between albedo and cloud fraction, however, the differences between the two datasets are small, and differences in linear slope are primarily found at midlatitudes (as stated above). Many models also have too-little spread in cloud fraction and underestimate the observed cloud fraction range. This concentration of points indicates too-little regional variability in model cloud distribution on the annual mean time scale.

The general characteristics of the latitudinal distribution are the same for models as for observations; that

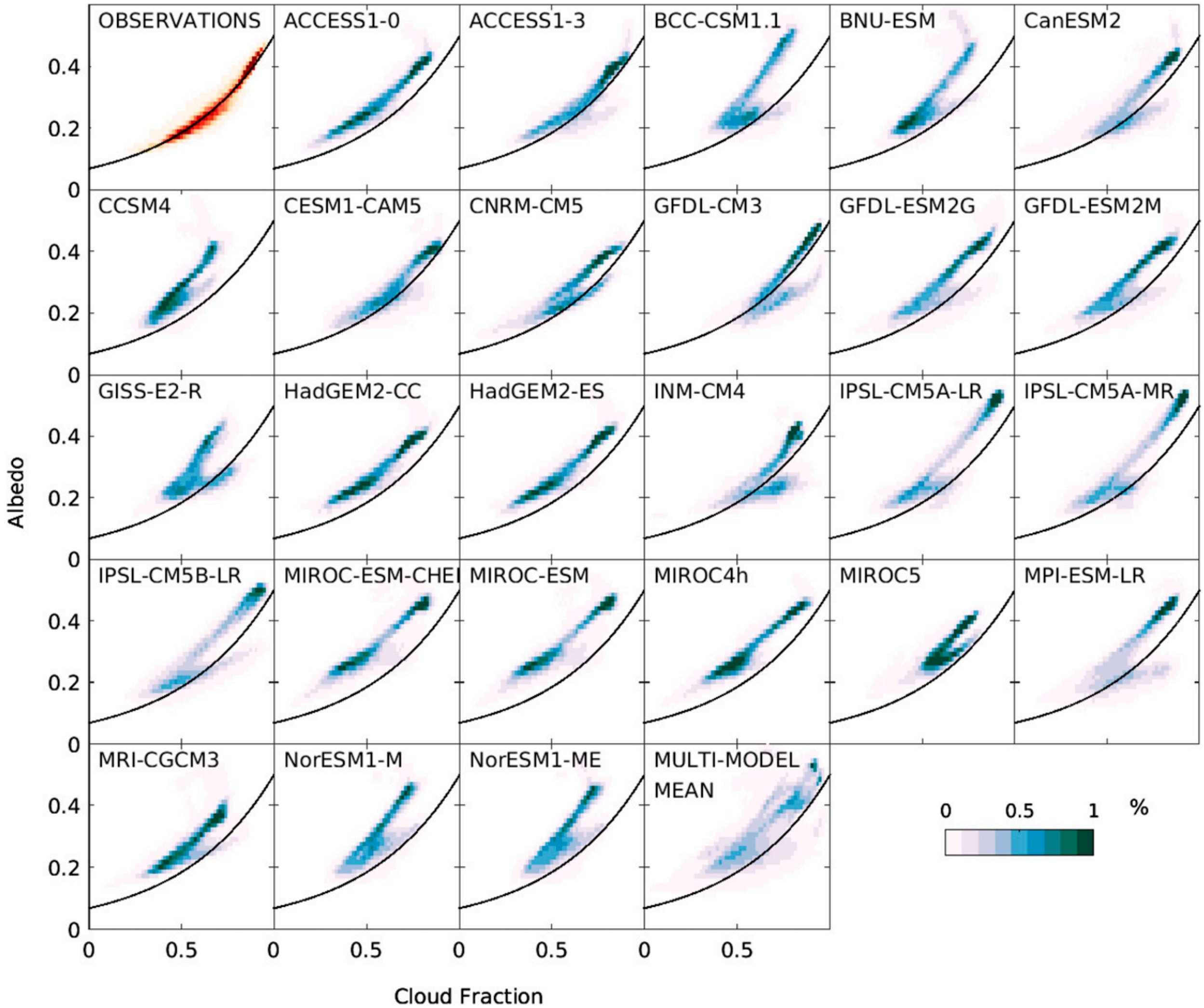

FIG. 3. Frequency of occurrence of each annually averaged cloud fraction–albedo combination, in percent of all cases for (top left) CERES and MODIS observations and individual CMIP5 models. Black lines represent the exponential fit to the near-global (60°S–60°N) satellite data, as in Fig. 1.

is, lower latitudes giving rise to a lower maximum and midlatitudes a higher maximum in the joint distribution of albedo and cloud fraction. Many models, however, do not reproduce the larger partial linear slope (corrected for SZA dependence) in the midlatitudes compared to the subtropics, seen in the observations (see Fig. 2), and the multimodel mean underestimates the slope for the midlatitude region. Also, whereas in the observations the different partial slopes align to a seemingly continuous distribution, many models show a branching, where one value of cloud fraction is not uniquely related to one value of albedo. Engström et al. (2015) showed some indication of this feature, but the annual mean time scale makes it more conspicuous. The branching is more or less clear in nearly all models, and the lower branch can be ascribed to tropical latitudes, for which the model slope is flatter than for subtropics and midlatitudes (see Fig. 2). Geographical mapping of the points contributing to the lower-albedo branch also shows good agreement with the observed distribution of cirrus clouds (Sassen et al. 2008), supporting the attribution of this branch to thin high clouds (see appendix B). Satellite simulators, representing active and passive sensors, also suggest that the branching is dependent on observational strategy (see appendix B), and the fact that the low albedo branch does not appear in CERES–MODIS observations may be a result of the failure of MODIS to detect optically thin clouds in the tropics, as discussed in section 2.

Compared to the observations, models tend to underestimate the slope in the tropics, and to a smaller degree in the midlatitudes, but display a less clear bias for the subtropics, where the multimodel mean also agrees well with observations. The model underestimate of the total albedo sensitivity to changes in cloud fraction in the tropics indicates that the composite of modeled clouds in the tropics is less reflective than in CERES–MODIS observations, although it has been shown that modeled low clouds in the tropics and subtropics are typically brighter than observed by *CALIPSO* (Nam et al. 2012). An overabundance of thin high clouds in the models or a failure of MODIS to properly retrieve those clouds would contribute to this apparent difference in model ability to represent the albedo of total and low cloud cover respectively.

The piecewise linear approximation to the relation between albedo and cloud fraction [Eq. (1)] used to define the slopes $d\alpha/df$ is found to be appropriate for all cases, with correlation coefficients between albedo and cloud fraction above 0.7 and slopes significantly greater than zero at the 95% confidence level. The one exception is the midlatitudes in MRI-CGCM, which displays the weakest model slope for that region in Fig. 2, where the correlation between albedo and cloud fraction is as low as 0.5.

b. Contrasting the NH and SH

Separating the NH and SH (up to 60° latitude) in observations, Figs. 1b,c show that the albedo–cloud fraction distributions are similar, the main difference being that the two local maxima are more clearly separated in the NH. In the SH the maximum related to lower-latitude clouds is less pronounced, and the maximum related to midlatitude clouds is more spread out. This difference in bimodality between NH and SH is more or less captured by the models; a majority of the models show two maxima more distinctly in the NH than in the SH. Further, the SH has a larger bright bias than the NH, and the branching in models, discussed in the previous section, is more prominent in the NH than the SH. The separate hemispheric distributions for all models and observations are displayed in appendix C.

From the previously documented symmetry between NH and SH in hemispheric mean total albedo, total reflection related to clouds may be expected to be greater in the SH than in the NH (Voigt et al. 2013; Stephens et al. 2015). This is consistent with the fact that the ocean-only 60°S–60°N subset of the global albedo is not hemispherically symmetric. For land and ocean, the NH (0°–60°N) albedo is approximately 5% greater, corresponding to a difference in reflected SW radiation of $4\,\mathrm{W\,m^{-2}}$, but for ocean only, where the higher frequency of relatively high-latitude ocean points in the SH also contributes to a higher mean value, the SH albedo (0°–60°S) is approximately 5% greater.

The models in general agree with these asymmetries in total albedo, with NH albedo on average 4% greater for 60°S–60°N land and ocean and SH albedo on average 3% greater for 60°S–60°N ocean only. For ocean only, one model (MRI-CGCM3) indicates a statistically significant (95%) reversed asymmetry, with larger NH albedo.

One possible explanation for a higher total albedo in the SH would be that SH clouds over the 60°S–60°N ocean are systematically brighter for a given cloud fraction. This is, however, not seen in the observations. Figure 4 (top left, observations), showing the ratio between relative frequency of occurrence of NH and SH points in albedo–cloud fraction space (i.e., accounting for the difference in land area between the hemispheres), does not indicate systematically brighter clouds in the SH. The SH dominates the very highest cloud fraction and albedo cases but also the lowest cloud fraction and albedo instances, indicating a greater total spatial variability of mean cloudiness in the SH. At the same time the lowest and highest albedo values for the intermediate cloud fractions are primarily found in the NH, indicating greater variability in albedo for a given cloud fraction, that is, more variable cloud albedo, in the NH.

The tendency for greater brightness bias in the SH is manifest in a majority of the models (Figs. C1 and C2). Figure 4 also shows a distinct SH dominance of higher-albedo cases and NH dominance of lower-albedo cases for a given cloud fraction, suggesting that many models, as well as the multimodel mean, in fact produce systematically brighter clouds in the SH. This feature is found to be most pronounced in the midlatitudes and subtropics.

c. Hemispheric differences by latitude

Separation of the latitude bands 0°–20°, 20°–40°, and 40°–60° in each hemisphere indicates a qualitative symmetry between the NH and SH with increasing cloud fraction and albedo sensitivity to cloud fraction with increasing latitude, as shown in Fig. 5. In both hemispheres, the midlatitudes include a cluster of points with lower cloud fraction and flatter slope that are not separable from the other points by latitudinal segregation. The influence of these points on the total midlatitude slope is greater in the NH than in the SH. Comparing observations to the multimodel mean (Fig. 6), we find that the models extend to lower cloud fractions, particularly in the subtropics, and most often overestimate the total albedo for a given cloud fraction and underestimate the cloud fraction for a given albedo. This is

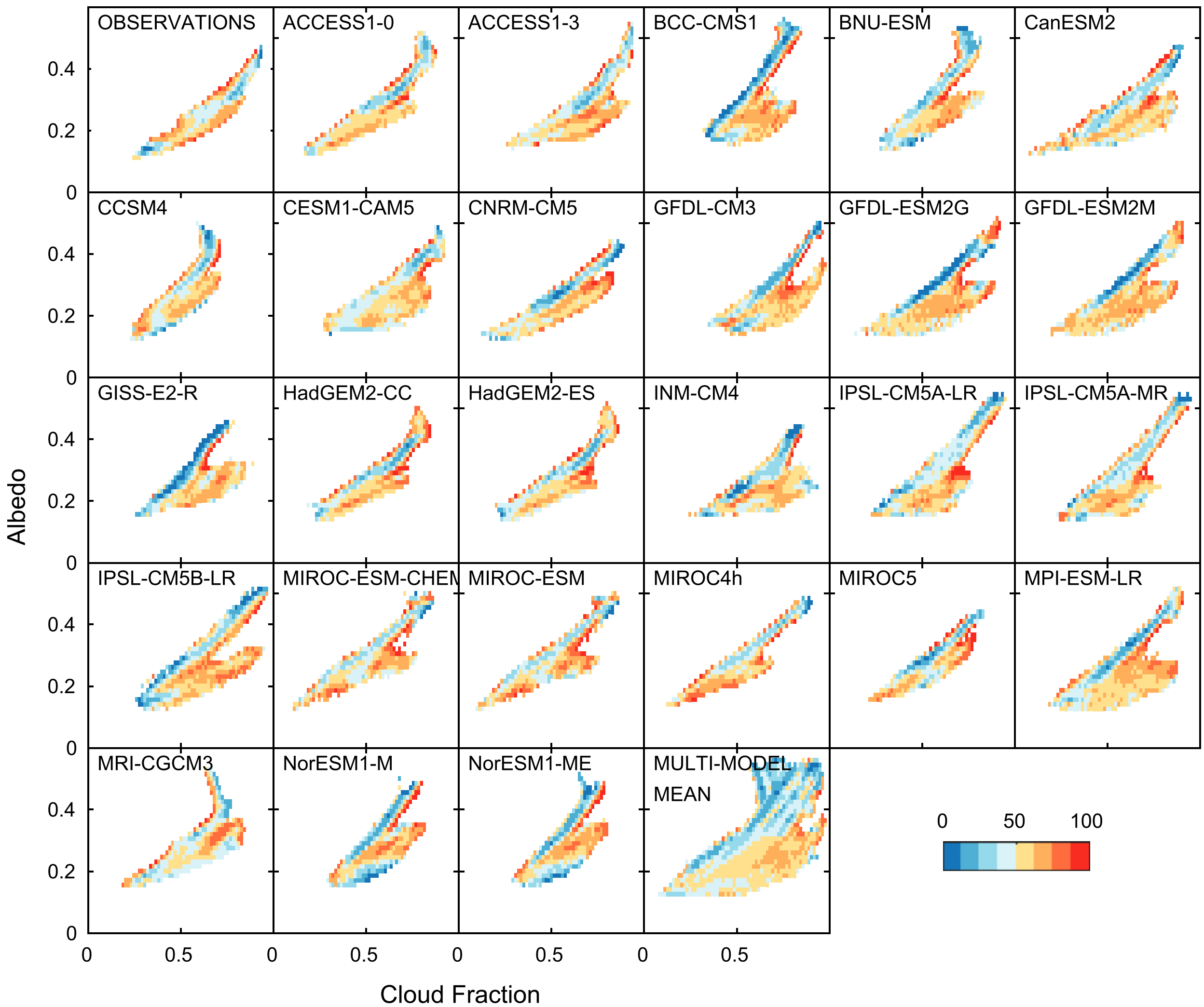

FIG. 4. Ratio between relative frequency of occurrence of points in albedo–cloud fraction space in NH and in SH. Color indicates percentage of points belonging to NH in each albedo–cloud fraction bin for (top left) CERES and MODIS observations and 26 CMIP5 models. Only points where relative frequency of occurrence for either hemisphere is greater than 0.01% are considered.

on the one hand consistent with model clouds being generally too few and too bright, as has been shown to be true for low clouds in the tropics and subtropics (Nam et al. 2012), compared to what is seen from *CALIPSO* observations, but on the other hand, as the composite of tropical clouds is found here to have smaller slope $d\alpha/df$ than MODIS observations and hence be less reflective than seen by MODIS, the general overestimation of brightness in models must partly be due to differences in clear-sky albedo. Regional mean clear-sky albedo is indeed found to be overestimated in almost all models, in agreement with Stevens (2015). As surface contributions to both all-sky and clear-sky albedo are small at these moderate latitudes (Donohoe and Battisti 2011; Stephens et al. 2015), this suggests a general overestimate of the atmospheric reflection for clear skies, again consistent with Stevens (2015), who attributes the difference in clear-sky albedo to a bias in aerosol reflection.

The importance of the clear-sky albedo bias is also enhanced by the fact that models in general have larger fractions of clear sky than observations. We acknowledge that satellite simulators should be used to support a quantitative comparison of cloud fraction between models and observations, but we find that overall, lower cloud fractions are overrepresented and higher cloud fractions underrepresented in models, particularly in subtropics and midlatitudes. This is consistent with, for example, Chepfer et al. (2013), who found that *CALIPSO* observations processed to be directly comparable to climate model output underestimate cloud fraction, particularly high- and midlevel clouds, compared

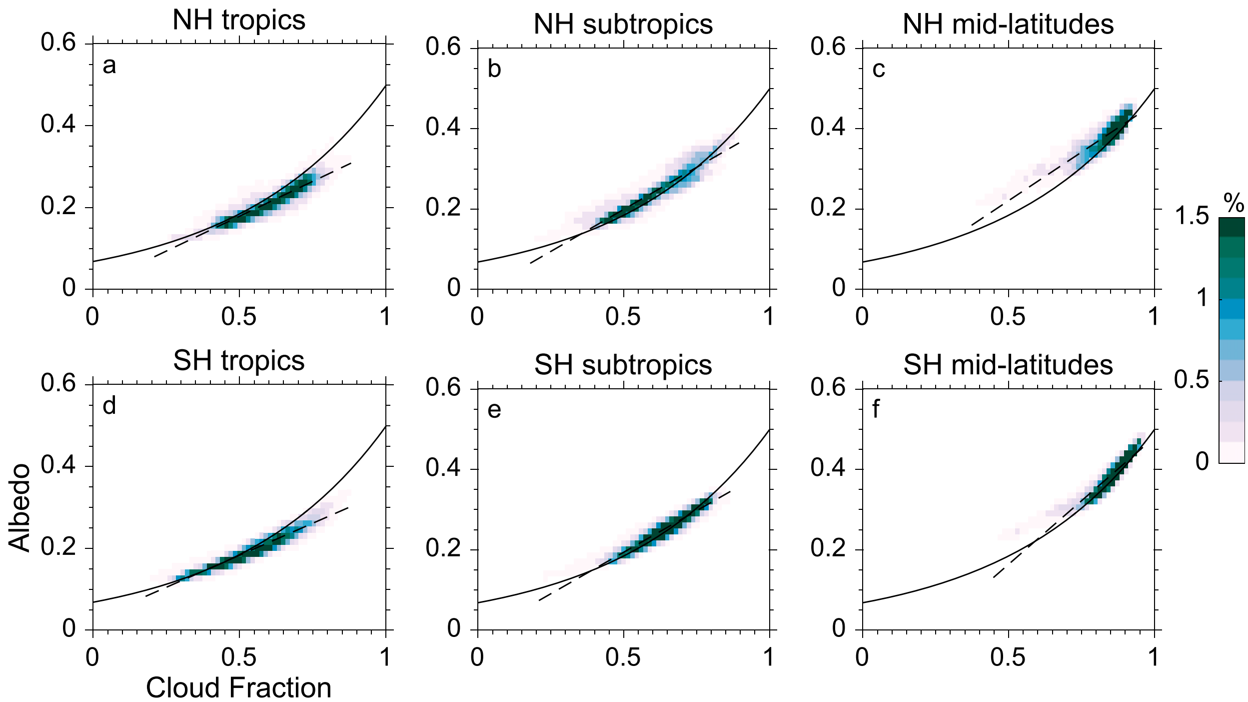

FIG. 5. Frequency of occurrence of each annually averaged observed (CERES and MODIS) cloud fraction–albedo combination, in percent of all cases in the given region for (a) NH tropics (0°–20°N), (b) NH subtropics (20°–40°N), (c) NH midlatitudes (40°–60°N), (d) SH tropics (0°–20°S), (e) SH subtropics (20°–40°S), and (f) SH midlatitudes (40°–60°S). Black solid lines represent the exponential fit to the near-global (60°S–60°N) satellite data, and dashed black lines represent linear fits to the displayed data.

to a higher-resolution *CALIPSO* product, and also with Jiang et al. (2012), who find that most CMIP5 models overestimate liquid water path compared to both passive and active satellite observations, indicating that model clouds are thicker, and accordingly fewer, than observed. However, as pointed out in section 2, the passive MODIS sensors are likely to underestimate the presence of optically thin clouds compared to active sensors like the lidar on *CALIPSO*, and the multimodel mean (Fig. 6) also indicates the more rare occurrence of higher cloud

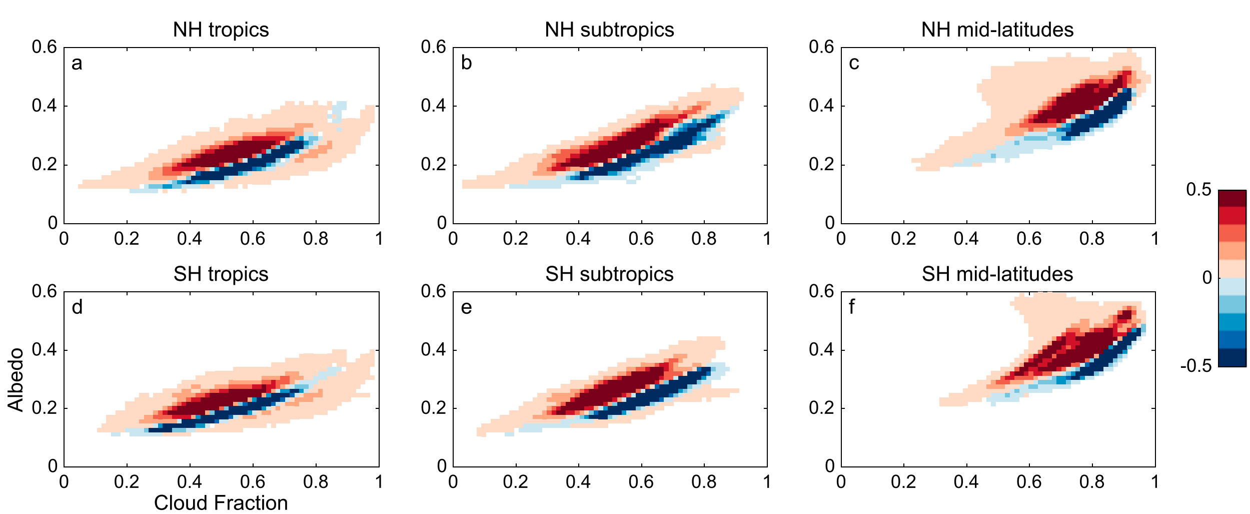

FIG. 6. Multimodel mean (26 CMIP5 models) difference in relative frequency of occurrence (in percent for consistency with Figs. 1 and 3) from observations (CERES and MODIS) for (a) NH tropics (0°–20°N), (b) NH subtropics (20°–40°N), (c) NH midlatitudes (40°–60°N), (d) SH tropics (0°–20°S), (e) SH subtropics (20°–40°S), and (f) SH midlatitudes (40°–60°S). Red colors indicate dominance of model points, and blue colors indicate dominance of observational points.

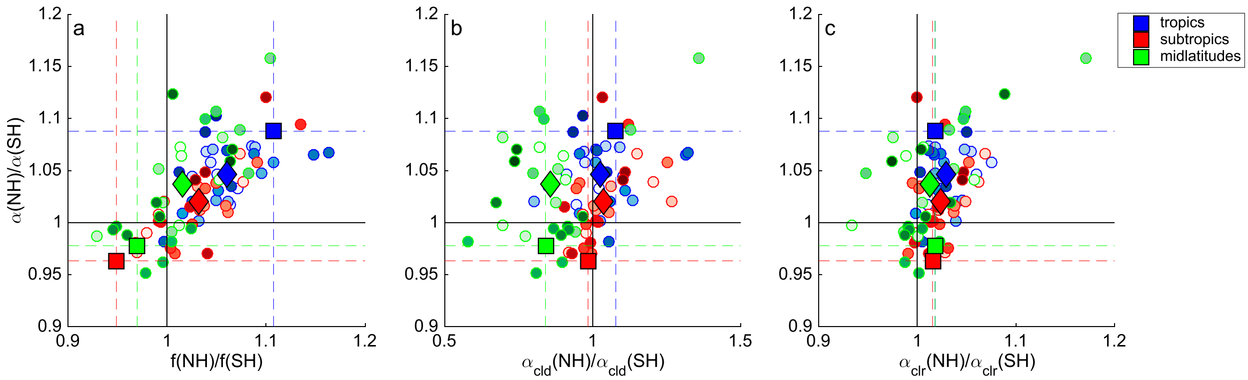

FIG. 7. NH–SH ratio for regional mean albedo α and its relation to NH–SH ratio for (a) f, (b) α_{cld}, and (c) α_{clr}, in 26 CMIP5 models and CERES and MODIS observations. Tropics (0°–20°), subtropics (20°–40°), and midlatitudes (40°–60°) are represented by blue, red, and green colors, respectively. Squares and dashed lines indicate observations, and diamonds indicate multimodel means. Individual models are represented by circles, colored as in Fig. 2. Note the difference in scale between α_{cld} and f and α_{clr}.

fraction and lower albedo in models in the tropics, resulting from the branching discussed in section 3a.

The low bias in model cloud fraction could potentially be reinforced by the midday sampling of the satellite observations, but replacing the SSF with the SYN product (see section 2) causes only a slight reduction in the ‘‘too few’’ bias at the highest cloud fractions in the midlatitudes.

Using the ratio between NH and SH regional averages of albedo, cloud fraction, cloud albedo, and clear-sky albedo we now evaluate the marine regional mean hemispheric asymmetry in models and observations in the separate latitude bands.

Cloud albedo α_{cld} is estimated from the partial linear slope $d\alpha/df$ in each region, according to Eqs. (1) and (2), where both the slope $d\alpha/df$ and the clear-sky albedo α_{clr} are corrected for SZA dependence on latitude based on RTM calculations as described in appendix A. NH midlatitude α_{cld} is not calculated for MRI-CGCM3, as the slope $d\alpha/df$ in this case cannot be differentiated from 0 at the 95% confidence level.

As seen from Figs. 7a–c (vertical axes), the asymmetry in albedo for the 60°S–60°N ocean-only subset of the globe is not evenly distributed with latitude. For the tropics (0°–20°) the observed albedo is higher in the NH than the SH (difference significant at the 99% level), and for the subtropics (20°–40°) and midlatitudes (40°–60°) regional mean albedo is higher in the SH than the NH, although these differences are significant only at the 80% level. Models agree with observations that the tropical NH has higher albedo than the tropical SH, which may be expected from the mean position of the ITCZ. Both NH and SH tropical mean albedo is overestimated in nearly all models (not shown), but models generally overestimate the albedo of the tropical SH more than that of the tropical NH, giving a smaller-than-observed NH–SH ratio, consistent with a spurious ITCZ in the SH in many models. For the subtropics and midlatitudes where the observations indicate higher albedo in the SH there is more disagreement among the models on which hemisphere has the highest albedo, but the multimodel mean in both cases indicates an NH–SH ratio greater than unity, in contrast with the observations.

The NH–SH ratio of total albedo in the three regions closely follows that of the NH–SH ratio of cloud fraction (Fig. 7a), in agreement with cloud fraction being the main driver of albedo variability (Loeb et al. 2007; George and Wood 2010; Engström et al. 2015). For the models the explained variance R^2 (based on all models and the three latitude bands) is 0.67. The NH–SH ratio of cloud albedo shows a larger spread between models (Fig. 7b), and here the correlation with NH–SH ratio in total albedo is weaker ($R^2 = 0.36$ for the models in the three latitude bands).

For tropical latitudes, the observed cloud fraction is higher in the NH compared to the SH (Fig. 7a, horizontal axis), and the estimated cloud albedo is also higher in the NH (Fig. 7b, horizontal axis), with differences significant at the 99% level, again in line with the mean position of the ITCZ. For midlatitudes, the SH shows higher cloud fractions as well as higher cloud albedo (differences significant at the 99% level), indicating more and brighter clouds than in the corresponding NH region, and for the subtropics cloud fraction is greater in the SH (difference significant at the 99% level), but cloud albedo appears hemispherically symmetric. This means that, to the extent that differences in cloud brightness compensate for lower surface and clear-sky albedo in the SH, this compensation seems to be taking place at midlatitudes rather than in the tropics or subtropics, at least for marine clouds.

For the tropics as well as the midlatitudes, the hemispheric asymmetries in cloud fraction and cloud albedo both contribute to the observed asymmetry in regional mean total albedo, while for the subtropics the asymmetries in regional mean albedo are primarily driven by the difference in cloud fraction between the hemispheres.

For the tropics, models agree with observations that the NH is cloudier, but most models underestimate the NH excess of cloudiness (Fig. 7a, horizontal axis). For the subtropics nearly all models have an NH excess in cloud fraction whereas observations indicate fewer clouds in the NH. For the midlatitudes the disagreement among models is greater, but almost all models show an NH excess or too-small SH excess in cloud fraction, compared to observations. Regional mean cloud fraction is strongly underestimated in many models, particularly in the midlatitudes and subtropics and typically more so in the SH (not shown). Again, a quantitative evaluation of cloud fraction would require applying appropriate satellite simulators to the models, output presently not supplied in the CMIP5 archive.

Similar to the observations, models indicate higher cloud albedo in SH midlatitudes compared to the NH counterpart, with the exception of the two GFDL models (Fig. 7b, horizontal axis). In the subtropics there is a tendency for NH cloud albedo to be higher, but the multimodel mean NH–SH ratio is close to 1. For the tropics, models disagree on the sign of the difference in cloud albedo between the two hemispheres. Most models underestimate the NH–SH ratio compared to observations, although the opposite behavior of the two MIROC-ESM models brings the multimodel mean NH–SH ratio close to the observed value. This means that the model underestimate of the cloud brightness in the tropical regions (section 3a) is stronger in the NH. The weaker asymmetry in tropical cloud brightness in models is consistent with the double-ITCZ problem, shifting the annual mean position of the ITCZ southward (Lin 2007; Oueslati and Bellon 2015).

For clear-sky albedo the variation between regions is small, and observed clear-sky albedo is consistently higher in the NH (Fig. 7c, horizontal axis), in accordance with higher aerosol loading in the NH (Loeb and Manalo-Smith 2005). The difference is, however, statistically significant only for the tropics (99% level), following the larger variability in subtropics and midlatitudes. The hemispheric asymmetry in clear-sky albedo is typically larger in models than in observations in accordance with Stevens (2015), although some models find the SH clear-sky albedo higher, particularly in the midlatitudes (notably, BNU-ESM, CCSM4, GISS-E2-R, and NorESM1-ME).

In short, Fig. 7 indicates that the asymmetry in total albedo over the ocean most closely follows the asymmetry in cloud fraction, and in the tropics and midlatitudes cloud albedo asymmetry also supports the asymmetry in total albedo. The asymmetry in clear-sky albedo is reproduced in the multimodel mean with largest intermodel variability in the midlatitudes, and for the total albedo, models typically underestimate the asymmetry in the tropics and show reversed asymmetry in the subtropics and midlatitudes compared to observations.

4. Summary

We present an evaluation of the relation between albedo and cloud fraction, on annual mean time scale over the near-global ocean (60°S–60°N), using 13 years of data from the satellite-based CERES and MODIS instruments and output from 26 CMIP5 models.

In the satellite observations, separating the tropics (0°–20°), subtropics (20°–40°), and midlatitudes (40°–60°) results in three separate populations within which the relation between albedo and cloud fraction is close to linear but that superimposed create a nonlinear distribution with two primary modes on the annual mean time scale. Tropical and subtropical clouds contribute to a regime of lower cloud fraction, lower albedo, and lower sensitivity of albedo to cloud fraction (comparatively dark/thin and scattered clouds), and midlatitude clouds result in a regime of higher cloud fraction, higher albedo, and higher sensitivity of albedo to cloud fraction (comparatively bright/thick and extensive cloud cover). The same separation into three latitude bands can be applied to the cloud population in global climate models with a similar result. Comparing models and observations on annual mean time scale, however, accentuates their differences.

The comparison between models and observations reveals a generally overestimated albedo at a given cloud fraction, which may be ascribed to a combination of overestimated cloud albedo and overestimated clear-sky albedo in the models. Models also generally underestimate cloud fraction, particularly in the subtropics and midlatitudes. Previous studies (e.g., Chepfer et al. 2013; Su et al. 2011) have indicated that active satellite instruments can observe clouds that are too optically thin to be simulated by models, which would lead to a model underestimate of cloud fraction. Given that active sensors are also able to identify thin cirrus clouds to a greater extent than passive sensors (e.g., Stubenrauch et al. 2013), the comparison with MODIS may actually offer a low estimate of the model bias in cloud fraction. The model underestimate of cloud fraction is also consistent with the ''too few, too bright'' problem previously identified in low-latitude, low-altitude clouds (Nam et al. 2012) but found by Klein et al. (2013) to be improved in CMIP5 models compared to previous-generation models.

For the tropics, however, models seem to capture thinner and lower-albedo clouds than MODIS. Models typically display a separate tropical branch in albedo–cloud fraction space, particularly conspicuous in the NH, with an underestimated sensitivity in total albedo to changes in cloud fraction, compared to CERES–MODIS observations. As MODIS observations are not able to retrieve the optically thinnest clouds, this branch of relatively high cloud fraction at low albedo may in fact to some degree be a realistic feature of the atmosphere. It is also possible that the models overestimate the amount of high thin clouds and their horizontal separation from lower and thicker clouds, yielding high cloud fractions at low albedo. Considering clouds as one extreme of a continuum in relative humidity distribution (Charlson et al. 2007), the fact that this combination of albedo and cloud fraction is frequent in models but not in observations points to the dependence of observational and simulated cloud fraction estimation on the definition of what a cloud is, as discussed in section 2.

We conclude that quantitative comparison of cloud fraction may be aided by the application of satellite simulators and welcome the inclusion of MODIS simulator output in coming climate model intercomparison projects.

Previous studies point out the symmetry in observed total albedo and absorbed SW radiation (Stephens et al. 2015; Voigt et al. 2013, 2014) as well as energy balance (Stephens and L'Ecuyer 2015) between the hemispheres. The fact that the NH and SH have practically the same total albedo, in spite of the brighter surface (resulting from more land) and greater atmospheric reflection (resulting from more aerosol) in the NH, indicates that the global cloud distribution compensates for the hemispheric differences in clear-sky albedo (i.e., that the SH has brighter and/or more clouds than the NH). Excluding land areas and latitudes above 60°, observations indicate that the SH is brighter by approximately $4\,\mathrm{W\,m^{-2}}$. For this subset of the global cloud scene, we use the relation between albedo and cloud fraction as a diagnostic tool, to assess the sources of asymmetry and differences between models and observations in this respect.

As may be expected from the hemispheric asymmetry in observed aerosol distribution (Loeb and Manalo-Smith 2005) the observed clear-sky albedo is consistently higher in the NH than the SH even when only ocean areas are considered. In the tropics this clear-sky albedo difference remains in the total albedo, and this is in fact the one region where albedo, cloud albedo, and cloud fraction are all higher in the NH. Hence, the tropical adjustments described by Hwang and Frierson (2013) and Voigt et al. (2014) are not sufficient to compensate for the asymmetry in clear-sky albedo. For subtropics and midlatitudes the clear-sky hemispheric bias is counteracted by cloud fraction and cloud albedo biases, and the total albedo is higher in the SH. The hemispheric asymmetry in total albedo is, however, most closely related to the hemispheric asymmetry in cloud fraction, in both models and observations.

Overall, the overestimation of albedo for a given cloud fraction in the models is greater in the SH than in the NH. The tendency for branched distributions, with a tropical branch with albedo closer to that observed, is also more pronounced in the NH. This, together with the double ITCZ contributes to a greater overestimate of total albedo in the tropical SH, acting toward closer hemispheric symmetry in this region, but the tropical NH still has higher albedo than the SH in models as well as in observations. In the subtropics and midlatitudes, where observations indicate higher albedo in the SH than the NH, a majority of the models show a weaker, or reversed, NH/SH bias.

The sensitivity of albedo to cloud fraction (linear slope) and estimated cloud albedo for midlatitude clouds is greater in the SH than in the NH in both observations and most models, indicating that these clouds may contribute to compensating for lower surface and clear-sky albedo in the SH. Contrarily for the tropics, observations indicate that cloud albedo is lower in the SH than in the NH, whereas models are not unanimous in this respect. For the subtropics the observations indicate similar cloud albedo in NH and SH, while models disagree on the sign of the bias. The ratio between NH and SH of cloud albedo in general displays larger variability between models than either cloud fraction or clear-sky albedo.

Models indicate higher tropical cloud fraction in the NH than the SH, in agreement with the observations. For subtropics and midlatitudes, observations indicate higher cloud fraction in the SH, acting to compensate for higher surface and clear-sky albedo in the NH. This is less well represented in the models that underestimate cloud fraction more in the SH than in the NH at these latitudes, even without inclusion of the high southern latitudes that have previously been pointed out as having underestimated cloud amount (Trenberth and Fasullo 2010; Hwang and Frierson 2013).

The higher cloud fraction and albedo in the tropical NH is expected from the mean position of the ITCZ, and the weaker asymmetry in models is consistent with the prevalent spurious double ITCZ residing in the SH.

Whereas the hemispheric asymmetry in clear-sky albedo is similar between models and observations, with greatest diversity in the midlatitudes, the model biases in regional mean albedo and cloud fraction in the tropics act almost exclusively toward closer hemispheric symmetry and for subtropics and midlatitudes toward weakened or reversed asymmetry compared to observations. For cloud albedo the model biases are more diverse.

The relationship between albedo and cloud fraction is a fundamental aspect of Earth's energy budget, which models should faithfully represent. We hope that the biases in individual models and the multimodel mean documented here can lead to improved representation of energy balance and cloud radiative properties in global models and to a better understanding of the role of clouds in Earth's albedo.

Acknowledgments. The authors thank the NASA Langley Atmospheric Science Data Center for satellite data distribution. We acknowledge the World Climate Research Programme's Working Group on Coupled Modelling, which is responsible for CMIP, and we thank the climate modeling groups (listed in Table 1 of this paper) for producing and making available their model output. For CMIP the U.S. Department of Energy's Program for Climate Model Diagnosis and Intercomparison provides coordinating support and led development of software infrastructure in partnership with the Global Organization for Earth System Science Portals. Funding for RW and RJC is provided by NASA Grant NNX13AQ35G. FB thanks the Fulbright commission, the Magnus Bergvall foundation, and Royal Swedish Academy of Sciences for contributions to a sabbatical leave at the University of Washington.

APPENDIX A

SZA Correction

A radiative transfer model (RTM) based on Corti and Peter (2009), with parameterization for clear-sky dependence on SZA taken from Cronin (2014), is used to account for the influence of solar zenith angle (SZA) on the apparent increase in albedo with increasing latitude. In the RTM, SW radiative fluxes are calculated based on a given MODIS-observed distribution of cloud fraction and cloud optical depth, under the plane-parallel assumption that is used in both satellite retrievals and climate models. This allows for quantification of the increase in clear-sky albedo and linear slope of the joint distribution of albedo and cloud fraction at a fixed cloud optical depth, which results from an increase in SZA only, and a subsequent scaling of the observed and modeled clear-sky and slope values to correspond to SZA 0. The ratio between SZA-determined slope $d\alpha/df$ or clear-sky albedo α_{clr} at a given SZA and at SZA 0 serves as a correction factor so that

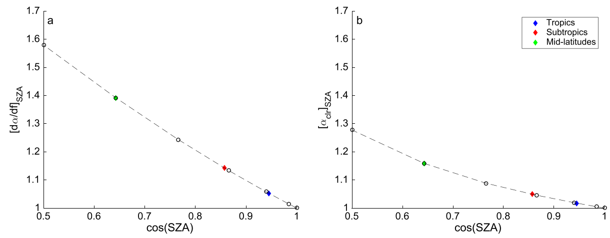

FIG. A1. (a) Dependence of linear slope $d\alpha/df$ on cos(SZA) at constant cloud optical depth (given by MODIS average from 60°S to 60°N), from RTM calculations of albedo, based on MODIS-observed cloud fraction. Slope values are given relative to slope at SZA 0°, and averaged cos(SZA) for the three latitude bands, tropics (0°–20°), subtropics (20°–40°), and midlatitudes (40°–60°), are marked with blue, red, and green color, respectively. (b) Corresponding dependence of α_{clr} on cos(SZA).

$$\frac{d\alpha}{df} = \frac{d\alpha/df^*}{(d\alpha/df)_{SZA}/(d\alpha/df)_0} \tag{A1}$$

and

$$\alpha_{clr} = \frac{\alpha^*_{clr}}{(\alpha_{clr})_{SZA}/(\alpha_{clr})_0}, \tag{A2}$$

where $d\alpha/df^*$ and α^*_{clr} refer to values not corrected for SZA dependence.

Figure A1 shows the SZA dependence of $d\alpha/df$ and α_{clr} according to the RTM, specifically indicating the correction factors corresponding to the mean (temporal and spatial) SZAs of the three latitude bands considered.

APPENDIX B

Low-Albedo Branch

The tropical region in a majority of the CMIP5 models creates a branch of lower albedo sensitivity to cloud fraction, alongside the higher albedo sensitivity for the

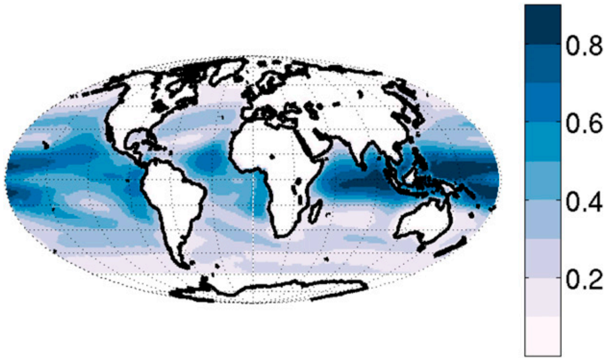

FIG. B1. Geographical distribution of the points creating a low-albedo branch in albedo–cloud fraction space in the CMIP5 models, shown as the multimodel mean fraction of occurrence of low-branch points in each 1° × 1° grid box, between 60°S and 60°N. Note that land-covered areas are excluded from the analysis.

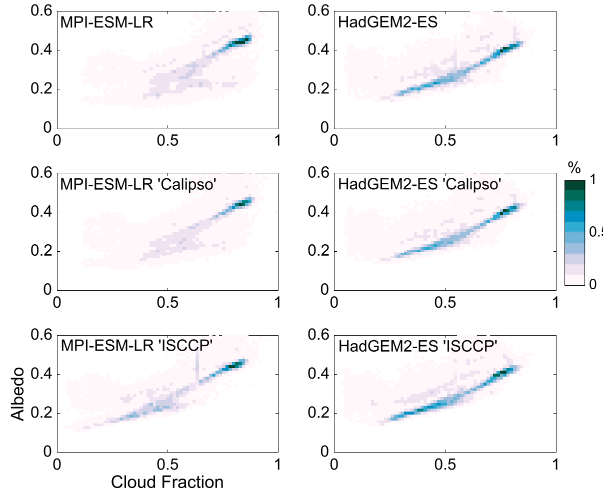

FIG. B2. Frequency of occurrence of each annually averaged cloud fraction–albedo combination for one year in percent of all cases for 60°S–60°N from (left) the MPI-ESM-LR, using (top) pure model cloud fraction, (middle) *CALIPSO* simulator cloud fraction, and (bottom) ISCCP simulator cloud fraction. (right) As in (left), but from the HadGEM2-ES.

same cloud fraction range resulting from higher-latitude clouds. To assess the geographical origin of the low-albedo branch, all points that fall below the partial linear slope for the subtropical region in each model are selected, and the multimodel mean relative occurrence of such points in each 1° × 1° grid box, between 60°S and 60°N is shown in Fig. B1. The pattern shows general agreement with the observed distribution of cirrus clouds (cf. Fig. 1 of Sassen et al. 2008).

The branching hence appears to be dependent on the detection of high thin clouds in the tropics, which may be inadequate for MODIS (see section 2). Figure B2 shows the distribution of annually averaged albedo and cloud fraction for two CMIP5 models (MPI-ESM-LR and HadGEM2-ES) using cloud fraction derived by the model and by satellite simulators mimicking the retrieval of cloud fraction for *CALIPSO* (active sensor) and ISCCP (passive sensors), respectively. For MPI-ESM-LR, the branch that is apparent in the model distribution is also clear when model albedo is combined with *CALIPSO* cloud fraction but much weaker for the ISCCP cloud fraction, and in HadGEM2-ES the branching does not appear in any of the cases. This indicates that even if the low-albedo branch were a reasonable feature of the real atmosphere, it may not be fully captured by the CERES–MODIS observations.

APPENDIX C

Hemispheric Joint Distributions

Figures C1 and C2 show the albedo–cloud fraction distributions in models and observations, separately for NH and SH (up to 60° latitude), respectively.

REFERENCES

Barker, H. W., G. L. Stephens, and Q. Fu, 1999: The sensitivity of domain-averaged solar fluxes to assumptions about cloud geometry. *Quart. J. Roy. Meteor. Soc.*, **125**, 2127–2152, doi:10.1002/qj.49712555810.

Barnes, W. L., T. S. Pagano, and V. V. Salomonson, 1998: Prelaunch characteristics of the Moderate Resolution Imaging Spectroradiometer (MODIS) on EOS-AM1. *IEEE Trans. Geosci. Remote Sens.*, **36**, 1088–1100, doi:10.1109/36.700993.

Bender, F. A.-M., R. J. Charlson, A. M.-L. Ekman, and L. Leahy, 2011: Quantification of monthly mean regional scale albedo of marine stratiform clouds in satellite observations and GCMs. *J. Appl. Meteor. Climatol.*, **50**, 2139–2148, doi:10.1175/JAMC-D-11-049.1.

Bodas-Salcedo, A., and Coauthors, 2011: COSP: Satellite simulation software for model assessment. *Bull. Amer. Meteor. Soc.*, **92**, 1023–1043, doi:10.1175/2011BAMS2856.1.

——, P. G. Hill, K. Furtado, K. D. Williams, P. R. Field, J. C. Manners, and P. Hyder, 2016: Large contribution of supercooled liquid clouds to the solar radiation budget of the Southern Ocean. *J. Climate*, **29**, 4213–4228, doi:10.1175/JCLI-D-15-0564.1.

Cess, R. D., 1976: Climate change: An appraisal of atmospheric feedback mechanisms employing zonal climatology. *J. Atmos. Sci.*, **33**, 1831–1843, doi:10.1175/1520-0469(1976)033<1831:CCAAOA>2.0.CO;2.

Charlson, R. J., A. S. Ackerman, F. A.-M. Bender, T. L. Anderson, and Z. Liu, 2007: On the climate forcing consequences of the albedo continuum between cloudy and clear air. *Tellus*, **59B**, 715–727, doi:10.1111/j.1600-0889.2007.00297.x.

Chepfer, H., G. Cesana, D. Winker, B. Getzewich, M. Vaughan, and Z. Liu, 2013: Comparison of two different cloud climatologies derived from CALIOP-attenuated backscattered measurements (level 1): The *CALIPSO*-ST and the *CALIPSO*-GOCCP. *J. Atmos. Oceanic Technol.*, **30**, 725–744, doi:10.1175/JTECH-D-12-00057.1.

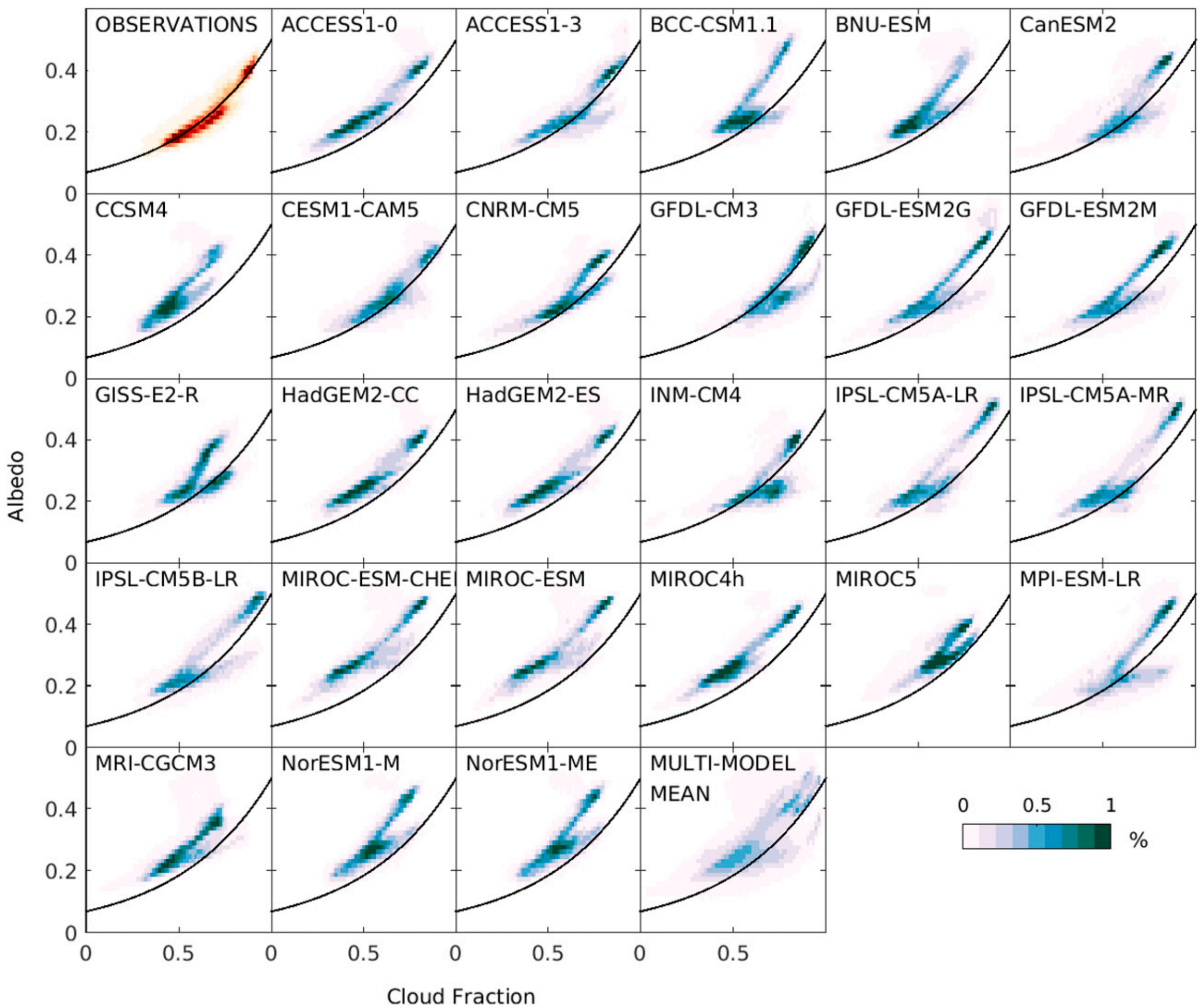

FIG. C1. Frequency of occurrence of each annually averaged cloud fraction–albedo combination in percent of all cases in the NH (0°–60°N) for (top left) CERES and MODIS observations and individual CMIP5 models. Black lines represent the exponential fit to the near-global (60°S–60°N) satellite data, as in Fig. 1.

Coakley, J. A., M. A. Friedman, and W. R. Tahnk, 2005: Retrieval of cloud properties for partly cloudy imager pixels. *J. Atmos. Oceanic Technol.*, **22**, 3–17, doi:10.1175/JTECH-1681.1.

Corti, T., and T. Peter, 2009: A simple model for cloud radiative forcing. *Atmos. Chem. Phys.*, **9**, 5751–5758, doi:10.5194/acp-9-5751-2009.

Cronin, T. W., 2014: On the choice of average solar zenith angle. *J. Atmos. Sci.*, **71**, 2994–3003, doi:10.1175/JAS-D-13-0392.1.

Donohoe, A., and D. S. Battisti, 2011: Atmospheric and surface contributions to planetary albedo. *J. Climate*, **24**, 4402–4418, doi:10.1175/2011JCLI3946.1.

Engström, A., F. A.-M. Bender, R. J. Charlson, and R. Wood, 2015: The nonlinear relationship between albedo and cloud fraction on near-global, monthly mean scale in observations and in the CMIP5 model ensemble. *Geophys. Res. Lett.*, **42**, 9571–9578, doi:10.1002/2015GL066275.

George, R. C., and R. Wood, 2010: Subseasonal variability of low cloud radiative properties over the southeast Pacific Ocean. *Atmos. Chem. Phys.*, **10**, 4047–4063, doi:10.5194/acp-10-4047-2010.

Hawcroft, M., J. M. Haywood, M. Collins, A. Jones, A. C. Jones, and G. Stephens, 2017: Southern Ocean albedo, inter-hemispheric energy transports and the double ITCZ: Global impacts of biases in a coupled model. *Climate Dyn.*, **48**, 2279–2295, doi:10.1007/s00382-016-3205-5.

Hwang, Y.-T., and D. M. W. Frierson, 2013: Link between the double-intertropical convergence zone problem and cloud biases over the Southern Ocean. *Proc. Natl. Acad. Sci. USA*, **110**, 4935–4940, doi:10.1073/pnas.1213302110.

Jiang, J. H., and Coauthors, 2012: Evaluation of cloud and water vapor simulations in CMIP5 climate models using NASA ''A-Train'' satellite observations. *J. Geophys. Res.*, **117**, D14105, doi:10.1029/2011JD017237.

Kay, J. E., C. Wall, V. Yettella, B. Medeiros, C. Hannay, P. Caldwell, and C. Bitz, 2016: Global climate impacts of fixing the Southern Ocean shortwave radiation bias in the

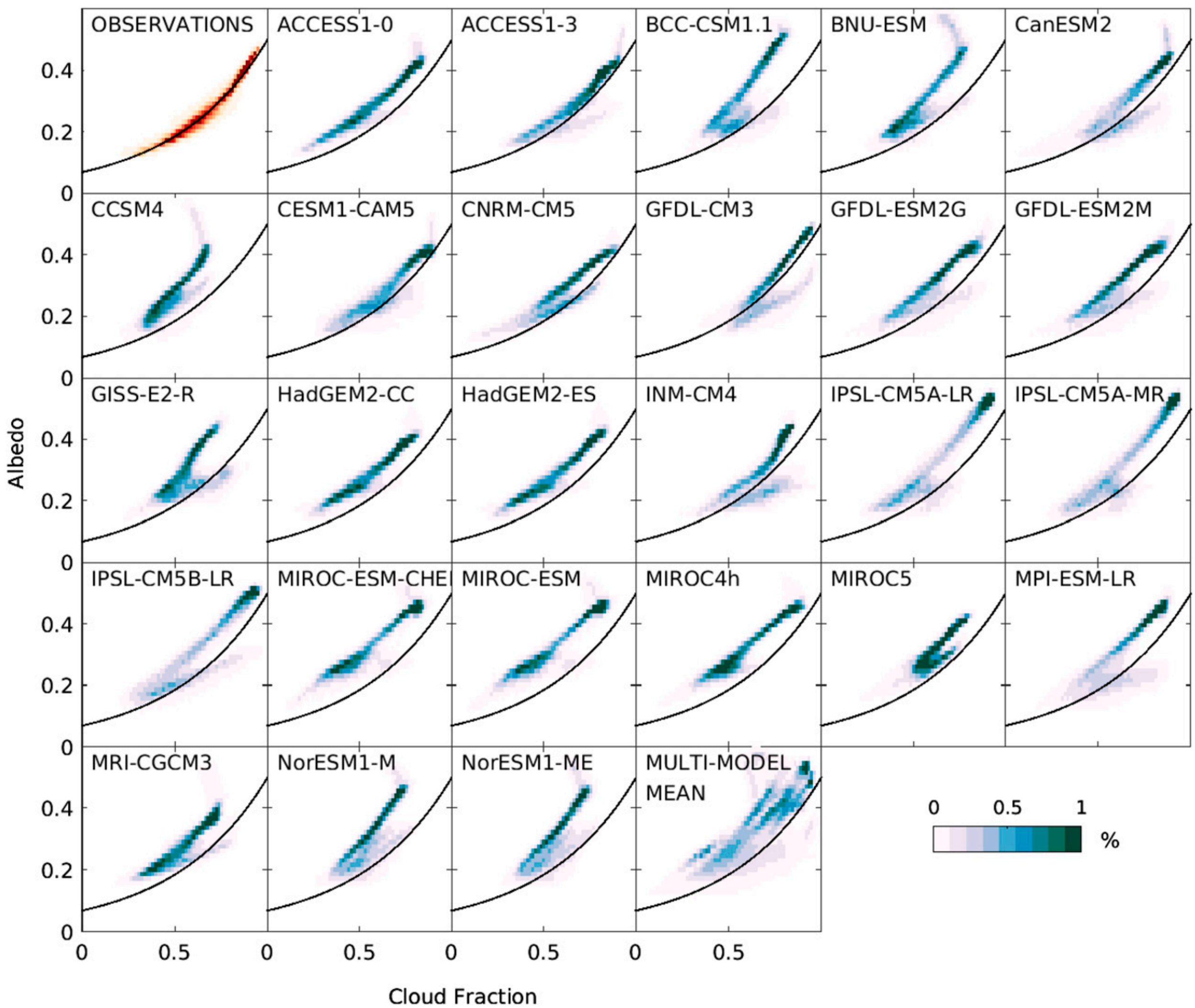

FIG. C2. As in Fig. C1, but for the SH.

Community Earth System Model (CESM). *J. Climate*, **29**, 4617–4636, doi:10.1175/JCLI-D-15-0358.1.

Klein, S. A., Y. Zhang, M. D. Zelinka, R. Pincus, J. Boyle, and P. J. Gleckler, 2013: Are climate model simulations of clouds improving? An evaluation using the ISCCP simulator. *J. Geophys. Res. Atmos.*, **118**, 1329–1342, doi:10.1002/jgrd.50141.

Liang, L., and L. Di Girolamo, 2013: A global analysis on the view-angle dependence of plane-parallel oceanic liquid water cloud optical thickness using data synergy from MISR and MODIS. *J. Geophys. Res. Atmos.*, **118**, 2389–2403, doi:10.1029/2012JD018201.

Lin, J.-L., 2007: The double-ITCZ problem in IPCC AR4 coupled GCMs: Ocean–atmosphere feedback analysis. *J. Climate*, **20**, 4497–4525, doi:10.1175/JCLI4272.1.

Loeb, N. G., and R. Davies, 1996: Observational evidence of plane parallel model biases: Apparent dependence of cloud optical depth on solar zenith angle. *J. Geophys. Res.*, **101**, 1621–1634, doi:10.1029/95JD03298.

——, and N. Manalo-Smith, 2005: Top-of-atmosphere direct radiative effect of aerosols over global oceans from merged CERES and MODIS observations. *J. Climate*, **18**, 3506–3526, doi:10.1175/JCLI3504.1.

——, S. Kato, K. Loukachine, and N. M. Smith, 2005: Angular distribution models for top-of-atmosphere radiative flux estimation from the Clouds and the Earth's Radiant Energy System instrument on the *Terra* satellite. Part I: Methodology. *J. Atmos. Oceanic Technol.*, **22**, 338–351, doi:10.1175/JTECH1712.1.

——, B. A. Wielicki, F. G. Rose, and D. R. Doelling, 2007: Variability in global top-of-atmosphere shortwave radiation between 2000 and 2005. *Geophys. Res. Lett.*, **34**, L03704, doi:10.1029/2006GL028196.

Marchand, R., T. P. Ackerman, M. Smyth, and W. B. Rossow, 2010: A review of cloud top heights and optical depth histograms from ISR, ISCCP, and MODIS. *J. Geophys. Res.*, **115**, D16206, doi:10.1029/2009JD013422.

McCoy, D. T., I. Tan, D. L. Hartmann, M. D. Zelinka, and T. Storelvmo, 2016: On the relationships among cloud cover, mixed-phase partitioning, and planetary albedo in GCMs. *J. Adv. Model. Earth Syst.*, **8**, 650–668, doi:10.1002/2015MS000589.

Minnis, P., and Coauthors, 2008: Cloud detection in nonpolar regions for CERES using TRMM VIRS and *Terra* and *Aqua* MODIS data. *IEEE Trans. Geosci. Remote Sens.*, **46**, 3857–3884, doi:10.1109/TGRS.2008.2001351.

——, and Coauthors, 2011: CERES edition-2 cloud property retrievals using TRMM VIRS and *Terra* and *Aqua* MODIS data. Part I: Algorithms. *IEEE Trans. Geosci. Remote Sens.*, **49**, 4374–4400, doi:10.1109/TGRS.2011.2144601.

Nam, C., S. Bony, J.-L. Dufresne, and H. Chepfer, 2012: The ''too few, too bright'' tropical low-cloud problem in CMIP5 models. *Geophys. Res. Lett.*, **39**, L21801, doi:10.1029/2012GL053421.

Oueslati, B., and G. Bellon, 2015: The double ITCZ bias in CMIP5 models: Interaction between SST, large-scale circulation and precipitation. *Climate Dyn.*, **44**, 585–607, doi:10.1007/s00382-015-2468-6.

Pincus, R., S. Platnick, S. A. Ackerman, R. S. Hemler, and R. J. P. Hofmann, 2012: Reconciling simulated and observed views of clouds: MODIS, ISCCP, and the limits of instrument simulators. *J. Climate*, **25**, 4699–4720, doi:10.1175/JCLI-D-11-00267.1.

Platnick, S., M. D. King, S. A. Ackerman, W. P. Menzel, B. A. Baun, J. C. Riédi, and R. A. Frey, 2003: The MODIS cloud products: Algorithms and examples from *Terra*. *IEEE Trans. Geosci. Remote Sens.*, **41**, 459–473, doi:10.1109/TGRS.2002.808301.

Sassen, K., Z. Wang, and D. Liu, 2008: Global distribution of cirrus clouds from *CloudSat*/*Cloud-Aerosol Lidar and Infrared Pathfinder Satellite Observations* (*CALIPSO*) measurements. *J. Geophys. Res.*, **113**, D00A12, doi:10.1029/2008JD009972.

Stephens, G. L., and T. L'Ecuyer, 2015: The Earth's energy balance. *Atmos. Res.*, **166**, 195–203, doi:10.1016/j.atmosres.2015.06.024.

——, D. O'Brien, P. J. Webster, P. Pilewski, S. Kato, and J.-I. Li, 2015: The albedo of Earth. *Rev. Geophys.*, **53**, 141–163, doi:10.1002/2014RG000449.

Stevens, B., 2015: Rethinking the lower bound on aerosol radiative forcing. *J. Climate*, **28**, 4794–4819, doi:10.1175/JCLI-D-14-00656.1.

Stubenrauch, C. J., and Coauthors, 2013: Assessment of global cloud datasets from satellites: Project and database initiated by the GEWEX radiation panel. *Bull. Amer. Meteor. Soc.*, **94**, 1031–1049, doi:10.1175/BAMS-D-12-00117.1.

Su, H., J. H. Jiang, J. Teixeira, A. Gettleman, X. Huang, G. Stephens, D. Vane, and V. S. Perun, 2011: Comparison of regime-sorted tropical cloud profiles observed by *CloudSat* with GEOS5 analyses and two general circulation model simulations. *J. Geophys. Res.*, **116**, D09104, doi:10.1029/2010JD014971.

Taylor, K. E., R. J. Stouffer, and G. A. Meehl, 2012: An overview of CMIP5 and the experiment design. *Bull. Amer. Meteor. Soc.*, **93**, 485–498, doi:10.1175/BAMS-D-11-00094.1.

Trenberth, K. E., and J. T. Fasullo, 2010: Simulation of present-day and twenty-first-century energy budgets of the southern oceans. *J. Climate*, **23**, 440–454, doi:10.1175/2009JCLI3152.1.

Voigt, A., B. Stevens, J. Bader, and T. Mauritsen, 2013: The observed hemispheric symmetry in reflected shortwave irradiance. *J. Climate*, **26**, 468–477, doi:10.1175/JCLI-D-12-00132.1.

——, ——, ——, and ——, 2014: Compensation of hemispheric albedo asymmetries by shifts of the ITCZ and tropical clouds. *J. Climate*, **27**, 1029–1045, doi:10.1175/JCLI-D-13-00205.1.

Vonder Haar, T. H., and V. E. Suomi, 1971: Measurements of the Earth's radiation budget from satellites during a five-year period. Part I: Extended time and space means. *J. Atmos. Sci.*, **28**, 305–314, doi:10.1175/1520-0469(1971)028<0305:MOTERB>2.0.CO;2.

Wielicki, B. A., B. R. Barkstrom, E. F. Harrison, R. B. Lee III, G. L. Smith, and J. E. Cooper, 1996: Clouds and the Earth's Radiant Energy System (CERES): An Earth observing system experiment. *Bull. Amer. Meteor. Soc.*, **77**, 853–868, doi:10.1175/1520-0477(1996)077<0853:CATERE>2.0.CO;2.

Winker, D. M., M. A. Vaughan, A. H. Omar, Y. Hu, K. A. Powell, Z. Liu, W. H. Hunt, and S. A. Young, 2009: Overview of the *CALIPSO* mission and CALIOP data processing algorithms. *J. Atmos. Oceanic Technol.*, **26**, 2310–2323, doi:10.1175/2009JTECHA1281.1.